Journal of the Korean Nuclear Society
Volume 26, Number 4, December 1994

《Techincal Report》

Drained End Shield Effects on Heat Deposition Rate Distribution in CANDU 6 Reactor End Shield Structure

Yung Kwon Jin, Kyo Youn Kim, and Hae Ryong Hwang
Korea Atomic Energy Research Institute
(Received August 5, 1994)

Abstract

The loss of water in the carbon steel balls and water region of the end shield for CANDU 6 reactor could lead to significant temperature gradient through the end shield structure which may result in the excessive deformation. With an assumed end shield drained scenario, the heat deposition rates were calculated through the end shield associated with the central fuel channel during full power operation as an initial step to thermal stress analysis. The drained case was compared with that of water present normal case in terms of heat deposition rates and the total heating throughout the end shield regions. The compared results show that the heat deposition and the total heating remain almost the same between the two cases. It was found that the change of volume integrated flux in the end shield regions due to the loss of water contribute a negligible effect on the heat deposition in this region.

1. Introduction

The end shield of CANDU 6 reactor[1] is a complex assembly of steel, water and fuel channel penetrations. The end shields are approximately 680cm diameter discs at either end of the reactor core. Each end shield has a 78.74cm region of carbon steel balls and light water sandwiched between a 5.08cm thick calandria side tube sheet and a 7.62cm thick fuelling machine side tube sheet, a total of 91.44cm. In each end shield, 380 fuel channel penetrations allow primary coolant to flow through the end shield to permit the refuelling operation. The fuel channel penetrations are arranged on 28.58cm square lattice of the reactor core and are formed by thin-wall lattice tube.

The carbon steel balls and water region consists of 60% carbon steel balls and 40% light water. This provides the biological shielding of radiation penetration from the core fuel region and the light water is circulated to remove the heat generated in and transferred to the end shield structure in normal operating condition[2]. If the loss of light water occurs in the end shield, due to break in the end shield supply headers, and assuming that the operator fails to respond to the alarms triggered by the low end shield level and flow during full power operation, then the end shields will heat up and eventually lead to dry out. Following the draining of the end shields, the fission power distribution in the reactor core remains unperturbed, and the reactor is assumed to operate at 100% full power. However, the loss of water shielding affects the radiation flux distribution. This could result in abnormal temperature gradients

in the end shield structure.

It is necessary to demonstrate that failures in this system do not lead to excessive deformations in the end shield structure which may affect the integrity of the fuel channel. The complete analysis sequence for this involves an initial consideration of heat generation rates, followed by the determination of steady state and transient heat transfer process, producing temperature distribution in the end shield structure, then finally an assessment of resultant stress and deformations. This paper deals only with the first aspect of the calculation chain. To this end, the heat deposition rate distribution was calculated through the end shield associated with the central fuel channel during full power operation for an assumed end shield drained scenario and compared to taht of the water present end shield case.

The two-dimensional discrete ordinate transport code DOT IV[3] was used to calculate the heat deposition rate distribution in the end shield regions. Since the heating rate becomes maximum in the central fuel channel, this channel was conservatively selected for this analysis. This calculation shows the axial heat distribution from the fuel regions throughout the end shield. The drained and the water present cases are compared in terms of heat deposition rate and total heating in each end shield components to assess the effects of the loss of water in the end shield. The heat distribution contributed by gammas and neutrons is provided in the three end shield regions, i.e., the calandria side tube sheet, the carbon steel balls and water region, and the fuelling machine side tube sheet. Also the total heating in these regions was calculated.

2. Source Distribution

CANDU 6 reactor contains 380 fuel channels which form a repeating array, therefore, the radiation transport through the end shield can be analyzed by using a radiation transport method with comprehensive two dimensional modelling capability. DOT IV was used to determine the radiation flux and heat distribution throughout the two-dimensional geometry system of the CANDU fuel channel, which used the reflective boundary condition at the start of Z axis and the end of R axis. The central fuel channel for which the channel power is 6.22 MW(th)[4] was conservatively chosen for this analysis and the 28.58cm square lattice pitch of fuel channel was modelled as 16.13cm radius of equivalent area to be represented in the R-Z geometry model.

The DOT IV code expects the radial and the axial fission density distributions in the source region. The source length was taken to be a two bundle length long fuel string (99.06cm) which is enough to predict the deeply penetrated radiation flux in the end shield region. The neighboring fuel channels and bundles beyond the two bundle long string were represented using reflective boundary condition.

2.1. Radial Fission Density Distribution

A 37 element fuel bundle contains a central fuel element, an inner ring (6 fuel elements), an intermediate ring (12 elements) and an outer ring (18 elements). In DOT IV analysis, each of those rings and the central elements was represented by two radial meshes. A total of 8 radial meshes were used to represent fuel bundle. The radial fission power distribution in the fuel bundle was based on the bundle power distribution of CANDU 6 fuel irradiated to an average exit burnup. According to this, the relative fissions in each fuel rings to that of the central element were estimated as follows[5]:

Central element	: 1.000
Inner ring	: 1.052
Intermediate ring	: 1.180
Outer ring	: 1.428

The fraction of total thermal power to total fission power is 0.955 for CANDU 6 reactor. If P represents the bundle thermal power in kW, P/0.955 gives the bundle fission power in kW. Then the average fission

density can be calculated by:

$$\frac{P\times 6.242\times 10^{15}}{0.955\times 206.1\times 2121} = 1.495\times 10^{10}P$$

[fissions · cm^{-3} · s^{-1}]

where 6.242×10^{15} = MeV · $s^{-1}kW^{-1}$,
206.1 = MeV/fission, and
2121 = volume of 37 fuel elements in cm^3 based on 49.53cm bundle length and a fuel element radius of 0.607cm.

The average of radial power distribution value is equal to 1.275, i.e., $(1.000+6\times 1.052+12\times 1.180+18\times 1.428)/37$. In consequences, the radial power distribution values are normalized as:

Central element: $1.495\times 10^{10}\ P\times 1.000/1.275 = 1.173\times 10^{10}\ P$

Inner Ring: $1.495\times 10^{10}\ P\times 1.052/1.275 = 1.233\times 10^{10}\ P$

Intermediate Ring: $1.495\times 10^{10}\ P\times 1.180/1.275 = 1.384\times 10^{10}\ P$

Outer Ring: $1.495\times 10^{10}\ P\times 1.052/1.275 = 1.674\times 10^{10}\ P$

Thus, the radial power factors incorporated into the DOT IV calculations are 1.173×10^{10} P, 1.233×10^{10} P, 1.384×10^{10} P, and 1.674×10^{10} P in units of fissions/cm-sec per kW thermal power.

2.2. Axial Fission Density Distribution

Since the radial power distribution was given in terms of fissions/cm sec per kW thermal power along the fuel string, the axial fission density distribution at the mesh mid points, where 14 meshes were used of the DOT IV calculations, was found in terms of thermal power in kW. This is based on the fission density distribution[6] calculated by ANISN[7] derived from the bundle thermal power in a central fuel channel[4] given in Table 1. The axial source distribution used in this analysis is given in Table 2.

Table 1. Bundle Thermal Powers Associated with a Central Fuel Channel

Mid-point of Fuel Bundle in Coordinate System of Figure 1 (cm)	Time Average Bundle Thermal Power (kW)
−272.4	726
−222.4	674
−173.4	600
−123.4	547
−74.3	403
−24.8	173

Table 2. Axial Power Shape Used in DOT4.2 Calculation

Mesh No.	Mesh Mid-point in Coordinate System of Figure 1 (cm)	Bundle Thermal Power (kW)
1	−95.5	475
2	−88.5	452
3	−81.4	428
4	−74.3	402
5	−67.2	374
6	−60.1	345
7	−53.1	314
8	−46.0	282
9	−38.9	247
10	−31.8	210
11	−24.8	172
12	−17.7	132
13	−10.6	91
14	−3.5	49

3. Group Structures, Cross-Sections, and Geometry Modelling

38 group energy scheme has been developed for these multigroup calculations, comprising 27 neutron groups coupled to 11 gamma groups. The number of neutrons per fission events were taken to be 2.62 [8]. The gamma groups include the prompt gammas from fission, the inelastic scatter gammas, and the

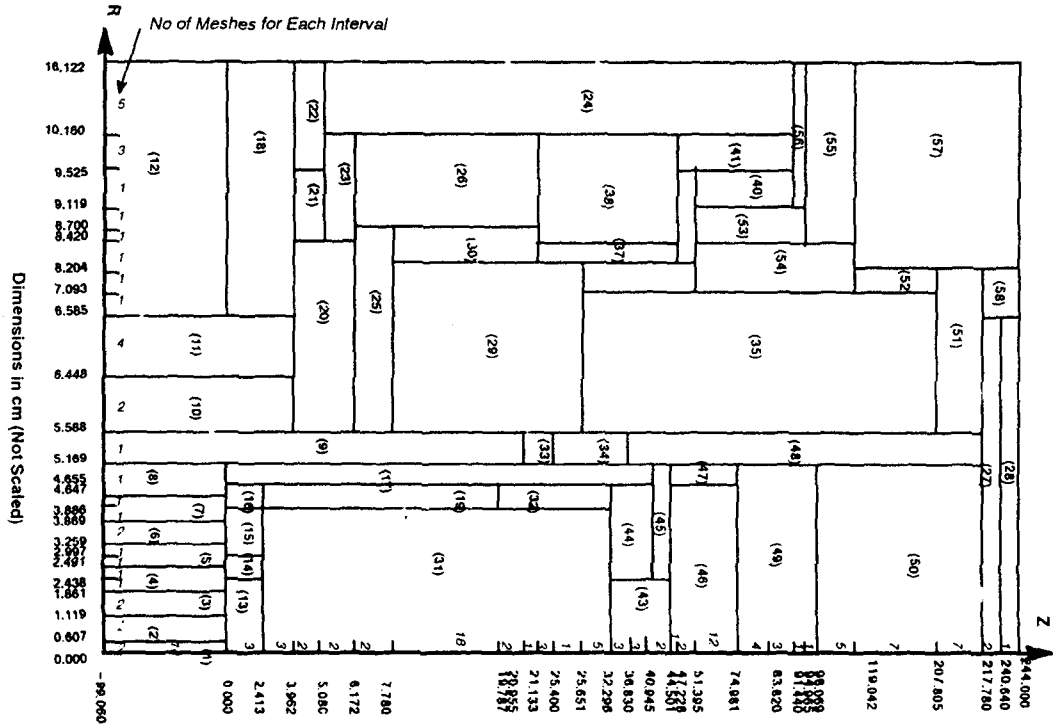

Fig. 1. Meah Structure used in DOT4.2 for Fuel Channel System

radiative capture gammas but exclude the fission product decay gammas. The fission product decay gammas, therefore, was included as a fixed source term, proportional to the fission power, with the gamma energy spectrum calculated and repartitioned gamma groups using the ORIGEN2 code[9]

Anisotropic scattering cross sections were expressed by means of a Legendre expansion which includes coefficients up to order of P_3. For the two-dimensional discrete ordinates calculation, a half-symmetric S_6 angular quadrature was utilized, such that at any mesh points, the angular variable was represented by 30 discrete directions[10,11]. The weighted difference model was used for the angular flux extrapolation across each mesh. The geometry and material models of the end shield components are shown in Figure 1 and Table 3.

4. Results and Discussions

The drained and water present case of axial variation of heat generation rates across the end shield, as a function of distance from the calandria side tube sheet up to fuelling machine side tube sheet is shown in Figure 2 to 4, which give the gamma, neutron, and total heating. As shown in these figures, the total heat distribution remains almost the same as the gamma heat distribution which is dominant over neutron heating. In the calandria side tube sheet region, the heat distribution between the two cases is almost the same. In carbon steel balls and water region, the heat in the inner region of the drained is lower than not drained case and becomes gradually higher as it goes outward to fuelling machine side tube sheet, which is not significant variation.

The total heating in the end shield components associated with a central fuel channel, with the drained and water present end shields, is presented in Table 4. This was obtained by the summation of

Table 3. Region Identification and Region Materials

No.	Region	Material
1	Central Fuel Pin	UO_2 Fuel
2	Coolant & Sheath	$Zr+D_2O$
3	Inner Fuel Annulus	UO_2 Fuel
4	Coolant & Sheath	$Zr+D_2O$
5	Intermediate Fuel Annulus	UO_2 Fuel
6	Coolant & Sheath	$Zr+D_2O$
7	Outer Fuel Annulus	UO_2 Fuel
8	Coolant & Sheath	$Zr+D_2O$
9	Pressure Tube	Zr
10	Annulus Gas	CO_2
11	Calandria Tube	Zr
12	Moderator	D_2O
13	Coolant	D_2O
14	Fuel Adaptor	SS410
15	Coolant	D_2O
16	Fuel Adaptor	SS410
17	Coolant	D_2O
18	Calandria Side Tube Sheet	SS304L
19	Shield Plug	SS410
20	Annulus Gas	CO_2
21	Lattice Tube	SS304L
22	Calandria Side Tube Sheet	SS304L
23	Lattice Tube	SS304L
24	End Shield	$SS410+D_2O$
25	Annulus Gas	CO_2
26	Lattice Tube	SS304L
27	Closure	SS403L
28	Air	Air
29	End Fitting	SS403L
30	Annulus Gas	CO_2
31	Coolant	D_2O
32	Side Plug Hole	$SS410+D_2O$
33	Liner Tube	SS410
34	Liner Tube Hole	$SS410+D_2O$
35	Coolant	D_2O
36	End Fitting	SS403L
37	Annulus Gas	CO_2
38	Lattice Tube	SS304L
39	Annulus Gas	CO_2
40	Annulus Gas	CO_2
41	Lattice Tube	SS304L
42	Fuelling Machine Side Tube	SS304L
43	Coolant	D_2O
44	Shield Plug	SS410
45	Shield Plug	SS410
46	Shield Plug	SS410
47	Coolant	D_2O
48	Lattice Tube	SS410
49	Shield Plug	SS410
50	Coolant	D_2O
51	End Fitting	SS403L
52	End Fitting	SS403L
53	End Fitting Sleeve	SS403L
54	End Fitting	SS403L
55	Air	Air
56	Air	Air
57	Air	Air
58	End Fitting	SS403L

the total heating in given mesh (viz., heating rates times mesh volumes) over all the meshes representing the component. The heat generation rates in the calandria side tube sheets constitute about 60% of the total heat load in the end shields. This heating is mainly due to prompt fission and capture gammas transported from the fuel and neutron capture gammas from the calandria side tube sheet. The heating in this component which is adjacent to the core end surface remained about the same as that of the water present. There is a slight reduction towards its outer surface due to absence of water in the end shields. The total heating in the carbon steel balls decreased by about 6.5% to a value of 763W. Total heating in the fuelling machine side tube sheet is negligible even in the case of drain in the carbon steel balls and water region. It should be noted that the total heating for the end shield components remained about the same as that of the heating during normal operations with the end shields not drained.

5. Conclusions

As the first step of thermal stress analysis for the end shield drain event, the heat deposition rate through the end shield structure was investigated between the drained and the water present cases. The heat deposition rates did not give significant differences between the two. It was also noted that

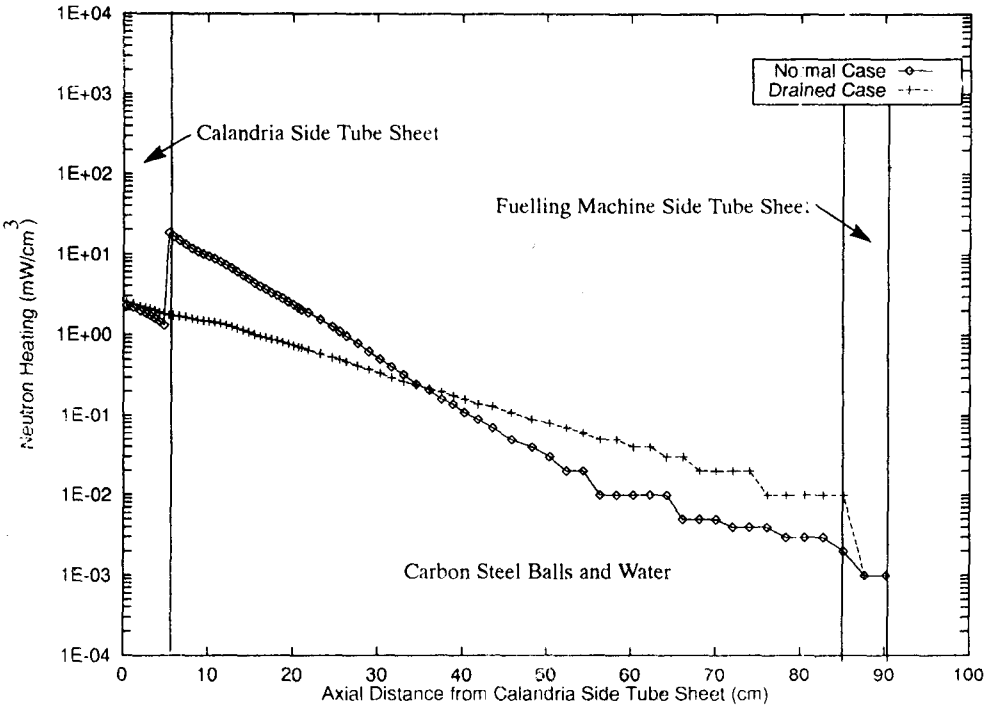

Fig. 2. Neutron Heat Distribution Across End Shield

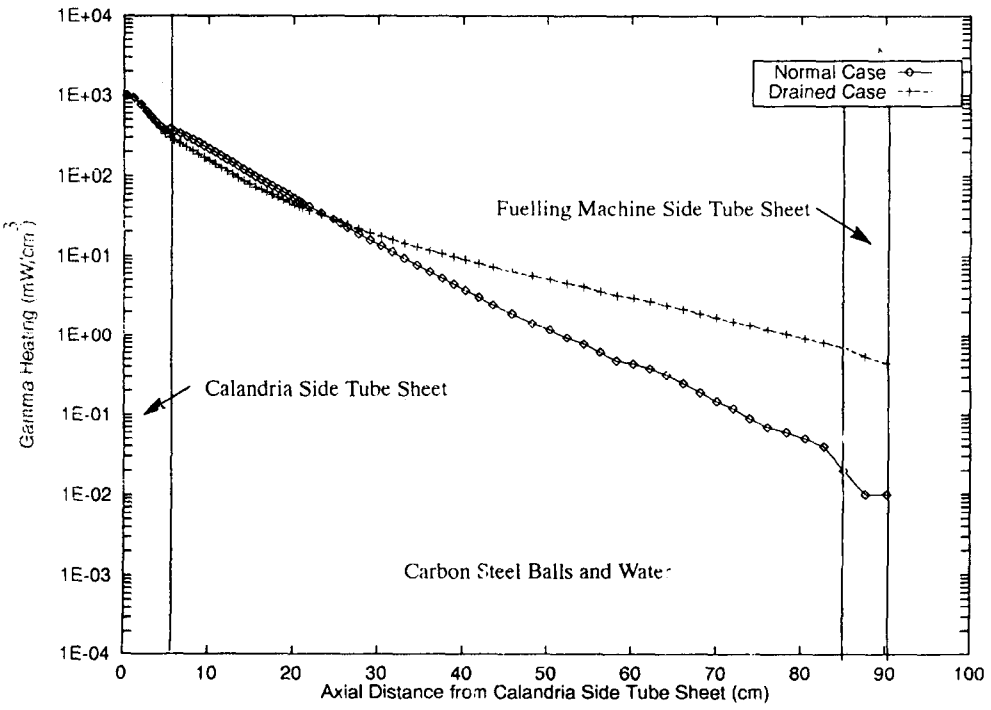

Fig. 3. Gamma Heat Distribution Across End Shield

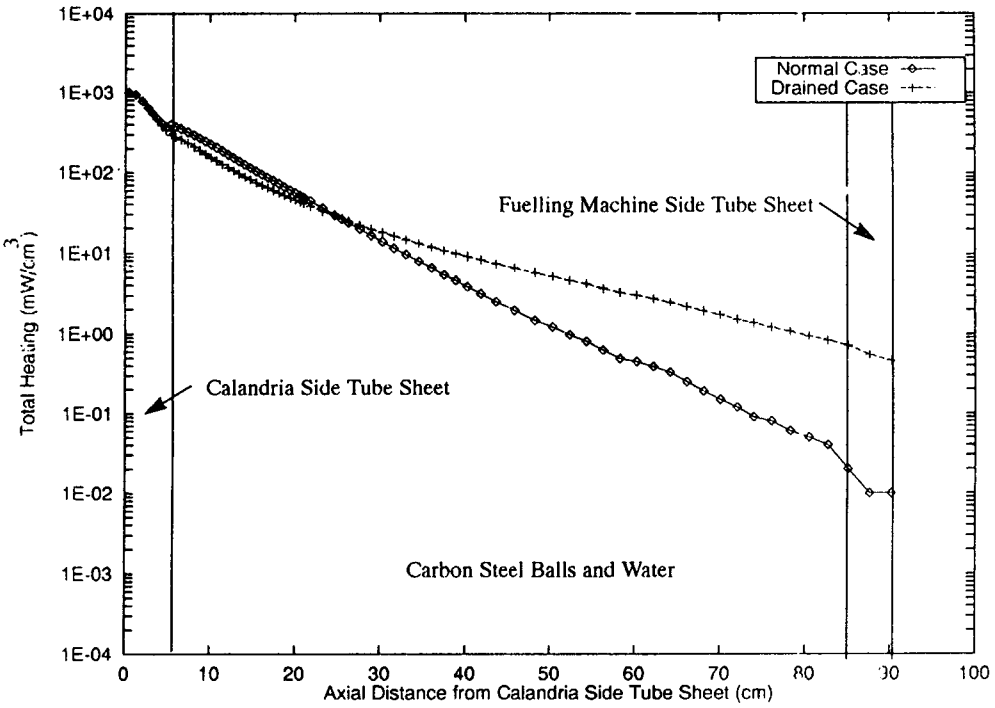

Fig. 4. Total Heat Distribution Across End Shield

Table 4. Total Heating in End Shield Components During Steady State and End Shild Drained State Operations.

Component	Component Volume (cm^3)	Total Heating (W)	
		End Shield Full	End Shield Drained
Calandria Side Tube Sheet	3.29E+3	2.30E+3	2.29E+3
Lattice Tube	5.86E+3	3.04+2	3.17E+2
End Fittings	1.73E+4	2.48E+2	2.83E+2
Carbon Sttel Balls and Water Region:			
Balls	2.48E+4	8.16E+2	7.63E+2
Water	1.65E+4	8.60E+1	None
Liner Tube	2.58E+3	7.00E+0	1.30E+1
Fuelling Machine Tube Sheet	3.75E+3	6.00E−2	2.20E+0

the total heating for the end shield components remained about the same as that of the heating with the end shields not drained. The heating has not changed significantly across the calandria side tube sheet in terms of its magnitude and the heat generation rates in the middle and outboard regions of the end shields are now higher than those with the water present case. In consequences, the loss of water in the end shields during normal operation should not result in significant heat distribution change compared with the water present end shields.

References

1. AECL, "Preliminary Safety Analysis Report for Wolsong Nuclear Power Plant Units 3 and 4," Korea Electric Power Corporation, 1992.
2. AECL, "Shield Cooling System Design Manual," 86-34110/63411-DM-000, 1993
3. W.A. Rhoades, D.B. Simpson, R.L. Childs, and W.W. Engle Jr., "DOT IV-Two Dimensional Discrete Ordinates Radiation Transport Code System", RSIC-CCC 320, Version 4.2, Oak Ridge National Laboratory, 1979.
4. M.A. Shad and H.C. Chow, "Fuel Management Report", 86-03310-AR-003, Atomic Energy of Canada Limited, Mississauga, Ontario, 1991.
5. I.E. Oldaker, "Fuel Design Manual," DM-59-37000, Atomic Energy of Canada Limited, Mississauga, Ontario, 1981.
6. K.Y. Kim and K. Aydogdu, "Radiation Heating Report," 86-03320-AR-004, Atomic Energy of Canada Limited, Mississauga, Ontario, 1993.
7. Westinghouse Astronuclear Laboratory and NASA Space Flight Center, "ANISN-W: Multigroup One-Dimensional Discrete Ordinates Transport Code with Anisotropic Scattering," RSIC-CCC-255, Oak Ridge National Laboratory, 1975.
8. G.D. Joanou and J.S. Dudek, "GAM-II, A B3 Code for the Calculation of Fast-Neutron Spectra and Associated Multigroup Constants," GA-4265, General Dynamics, 1963.
9. A.G. Croff, "ORIGEN2-Isotope Generation and Depletion Code-Matrix Exponential Method," RSIC-CCC-371, Oak Ridge National Laboratory, 1980.
10. J.P. Jenal, P.J. Erickson, W.A. Rhodes, D.B. Simpson, and M.L. Wiliams, "The Generation of Computer Library for Discrete Ordinates Quadrature Set," ORNL/TM-6023, Oak Ridge National Labratory Report1, 1977.
11. W.A. Rhoades, "The DOT IV Variable Mesh Discrete Ordinates Transport Codes," Proceeding of the Fifth International Conference on Reactor Shielding, April 18-23, 1977.